
Intersection Regularization for Extracting Semantic Attributes

Ameen Ali¹ Tomer Galanti¹ Evgeniy Zheltonozhskiy² Chaim Baskin² Lior Wolf¹

Abstract

We consider the problem of supervised classification, such that the features that the network extracts match an unseen set of semantic attributes, without any additional supervision. For example, when learning to classify images of birds into species, we would like to observe the emergence of features that zoologists use to classify birds. We propose training a neural network with discrete top-level activations, which is followed by a multi-layered perceptron (MLP) and a parallel decision tree. We present a theoretical analysis as well as a practical method for learning in the intersection of two hypothesis classes. Since real-world features are often sparse, a randomized sparsity regularization is also applied. Our results on multiple benchmarks show an improved ability to extract a set of features that are highly correlated with the set of unseen attributes.

1. Introduction

The extraction of meaningful intermediate features in classification problems is at the heart of many scientific domains. Such features allow experts to discuss a certain classification outcome and help understand the classification problem’s underlying structure. In botany, the species are often identified based on dichotomous keys related to the shape of the leaf, the texture of the fruit, etc. (Herbarium, 2013). In paleography, the manuscript is dated or attributed to a specific scribe, based, for example, on specific characteristics of the morphology of the letters (Stokes, 2009).

The mid-level attributes we discuss are binary and need to be both evidence-based and distinctive. The first property means that there is a mapping f such that every input x is mapped to a vector $f(x)$ of binary values, indicating the presence of each attribute. The second property means that there should be simple rules that determine the class label

$y(x)$ based on the obtained attributes $f(x)$.

Currently, deep neural networks are the leading methodology for obtaining attributes from images in a repeatable way (Zhang et al., 2014; Xu et al., 2020) and for classification. Decision trees with binary decision stumps are a leading way for obtaining simple and interpretable decision rules based on attributes (Guidotti et al., 2018). We propose to learn a deep neural network, such that the learned quantized representation is suitable for classification by an MLP, as well as by a decision tree.

To perform this hybrid learning task, we provide a theoretical analysis of the problem of learning at the intersection of two hypothesis classes. We study the optimization dynamics of training two hypotheses from two different classes of functions. The first one is trained to minimize its distance from the second one, and the second one is trained to minimize its distance from the first one and the target function. We call this process *Intersection Regularization*, as it regularizes the second hypothesis to be close to the first hypothesis class. We theoretically discuss the conditions on the loss surface, for which this process converges to an equilibrium point or local minima.

The method that we develop for concurrently training a network and a tree is based on the proposed analysis. We train a quantized representation of the data and two classifiers on top of it: a decision tree and multi-layered perceptron (MLP). The two classifiers are trained using intersection regularization. Since many of the human-defined attributes are relatively spares, we also apply L_1 regularization on the quantized vector of activations.

In an extensive set of experiments, we demonstrate that learning with this method produces a set of quantized activations that is enriched with decision stumps that are highly correlated with a set of human-defined attributes, which were kept unseen during training. This is at the expense of a slight reduction in the overall classification accuracy compared to training the network without the proposed loss functions.

The central contributions in this paper are as follows:

1. We identify a novel learning problem that we call *Unsupervised Recovery of Semantic Attributes*. In this

*Equal contribution ¹School of Computer Science, Tel Aviv University, Tel Aviv, Israel ²Department of Computer Science, Technion, Haifa, Israel. Correspondence to: Tomer Galanti <tomert2g@gmail.com>.

setting, the samples are associated with abstract binary attributes and are labeled by class membership. The algorithm is provided with labeled samples and is judged by the ability to recover the binary attributes without any access to them. We provide concrete measures for testing the success of a given method for this task.

2. We introduce a method for recovering the semantic attributes. This method is based on a novel regularization process for regularizing a neural network using a decision tree. We call this regularization method, ‘*Intersection Regularization*’.
3. We theoretically study the convergence guarantees of the new regularization method to equilibrium points and local minima.

2. Related Work

We list various approaches for learning explainable models in the literature and discuss their similarities and dissimilarities with our approach.

Interpretability Developing tools and techniques to better interpret existing deep learning based approaches and to that end building explainable machine learning algorithms, is a fast-growing field of research. In computer vision, most contributions are concerned with providing an output relevance map. These methods include saliency-based methods (Dabkowski & Gal, 2017; Simonyan et al., 2013; Mahendran & Vedaldi, 2016; Zhou et al., 2016a; Zeiler & Fergus, 2014; Zhou et al., 2018; Gur et al., 2020), Activation Maximization (Erhan et al., 2009) and Excitation Backprop (Zhang et al., 2018), perturbation based methods (Fong et al., 2019; Fong & Vedaldi, 2017). Shapley-value based methods (Lundberg & Lee, 2017) enjoy theoretical justification and the Deep Taylor Decomposition (Montavon et al., 2017) provides a derivation that is also applicable to Layer-wise Relevance Propagation (LRP) (Bach et al., 2015) and its variants (Gu et al., 2018; Iwana et al., 2019; Nam et al., 2019) presented RAP. Gradient based methods are based on the gradient with respect to the layer’s input feature map and include Gradient*Input (Shrikumar et al., 2016), Integrated Gradients (Sundararajan et al., 2017), SmoothGrad (Smilkov et al., 2017), FullGrad (Srinivas & Fleuret, 2019) and Grad-CAM (Selvaraju et al., 2017).

This approach suffers from several notable disadvantages. First, many of these methods were shown to suffer from a bias toward image edges and fail sanity checks that link their outcome to the classifier (Asano et al., 2019). Furthermore, even though these methods are useful for visualization and downstream tasks, such as weakly supervised segmentation (Li et al., 2018), it is not obvious how to translate the image maps produced by these methods into semantic attributes, i.e., extract meaning from a visual depiction. An

additional disadvantage of this approach is that it does not provide a direct method for evaluating whether a given neural network is interpretable or not and the evaluation is often done with related tasks, such as segmentation or on measuring the classifier’s sensitivity to regions or pixels that were deemed as being important to the classification outcome or not. In our framework, we suggest objective measures in which one is able to quantify the degree of interpretability of a given model.

Since linear models are intuitively considered interpretable, a framework in which the learned features are monotonic and additive has been developed (Alvarez-Melis & Jaakkola, 2018a). The explanation takes the form of presenting each attribute’s contribution, while explaining the attributes using prototype samples. Unlike our framework, no attempt was made to validate that the obtained attributes correspond to a pre-defined list of semantic attributes.

Local interpretability models, such as LIME (Ribeiro et al., 2016), approximate the decision surface for each specific decision by a linear model and are not aimed at extracting meaningful attributes as in our method. Besides, such models are known to be sensitive to small perturbations of the input (Yeh et al., 2019; Alvarez-Melis & Jaakkola, 2018b).

Fine-Grained Classification Fine-grained classification aims at differentiating subordinate classes of a common superior class. Those subordinate classes are usually defined by domain experts, based on complicated rules, which typically focus on subtle differences in particular regions. Because of the inherent difficulty in classifying slightly different classes, many contributions in this area often aim at detecting informative regions in the input images that aid in classifying them (Chen et al., 2019; Yang et al., 2018; Huang & Li, 2020; Hu et al., 2019; Zhuang et al., 2020). In our work, we would like to recover semantic attributes that are not necessarily associated with specific image regions, e.g., mammal/reptile, omnivore/carnivore.

Explainability of Decision Trees Decision trees are known to be naturally explainable models, as long as the decision rules are easy to interpret. However, as far as we know, it was not shown before that learning trees, while optimizing the features leads to the emergence of attributes of a large set of relevant attributes.

In the context of recommendation systems interpretability, metatrees were used for providing per-user decision rules (Shulman & Wolf, 2020). This method relies on a pre-existing set of features rather than extracting them from the input. Another line of work (Frosst & Hinton, 2017), which also employs preexisting features, distills the information in a deep network into a soft decision tree (Irsoy et al., 2012). Unlike our work, the neural network is not optimized to produce suitable features.

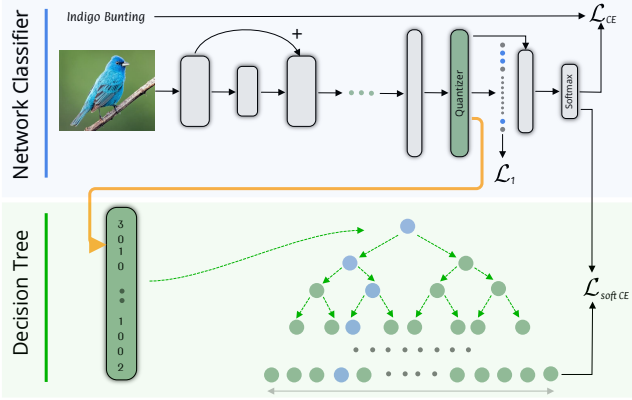


Figure 1. An illustration of the method in Sec. 5. The model has three main components: (a) a quantized representation function F_q , (b) a classifier neural network G and (c) a multivariate decision tree T . We have three losses: a L_1 regularization over the masked quantized features, a cross entropy loss between the network and the ground-truth labels and a soft cross entropy loss between the outputs of the tree and the network.

More relevant to our work is the one of the Adaptive Neural Trees method (Tanno et al., 2019), which also combines decision trees and neural networks. In this method, trees of dynamic architectures that include network layers are grown so that the underlying network features gradually evolve. It is shown that the learned tree divides the classes along meaningful axes but the emergence of semantic attributes was not shown.

Quantization Quantization is the conversion of the floating-point data to low-bit discrete representation. The most common approaches for training a quantized neural network employs two sets of weights (Hubara et al., 2018; Zhou et al., 2016b). The forward pass is performed with quantized weights, and updates are performed on full precision ones, i.e., approximating gradients with the straight-through estimator (STE) (Bengio et al., 2013). In this work, we make use of quantizations in order to learn discrete, interpretable representations of the data within a neural network.

3. Problem Setup

In this section, we formulate a new learning setting that we call *Unsupervised Recovery of Semantic Attributes*. In this setting, there is an unknown target function $y : \mathcal{X} \rightarrow \mathcal{Y}$ along with an attributes function $f : \mathcal{X} \rightarrow \mathcal{U}^d$ that we would like to learn. Here, $\mathcal{X} \subset \mathbb{R}^n$ is a set of instances and \mathcal{Y} is a set of labels. The function f is assumed to be d_0 -sparse, i.e., $\forall x \in \mathcal{X} : \|f(x)\|_0 \leq d_0$. The values of f are taken from a latent space \mathcal{U}^d , where $\mathcal{U} = \mathbb{R}, [-1, 1]$ or $\{\pm 1\}$, depending on the task at hand.

For example, \mathcal{X} can be a set of images of k animal species and $\mathcal{Y} = \{e_i\}_{i=1}^k$ is the set of labels, where $e_i \in \mathbb{R}^k$ is the

i 'th elementary vector. In this case, y is a classifier that takes an animal image x and returns the class in which this animal belongs to. The function f corresponds to a set of d binary attributes $\{f_i\}_{i=1}^d$ (i.e., carnivore/herbivore, etc'). Each attribute f_i takes an image x and returns whether the animal illustrated in x satisfies this attribute $f_i(x) \in \{0, 1\}$.

Similar to the standard learning setting, the set \mathcal{X} is endowed with a distribution D , from which samples x are being taken. The learning algorithm is provided with a set $\mathcal{S} = \{(x_i, y(x_i))\}_{i=1}^m$ of m i.i.d. samples. In the standard learning setting, the learning algorithm is supposed to fit a hypothesis $H : \mathcal{X} \rightarrow \mathcal{Y}$ from a given hypothesis class \mathcal{H} that would minimize the *expected risk*:

$$\mathcal{L}_D[H, y] := \mathbb{E}_{x \sim D}[\ell(H(x), y(x))], \quad (1)$$

where $\ell : \mathcal{Y}^2 \rightarrow [0, \infty)$ is some loss function, for example, the ℓ_2 loss function $\ell_2(a, b) = \|a - b\|_2^2$ for regression or the cross-entropy loss for classification. Since the algorithm is not provided with a full access to D , the algorithm typically minimizes the empirical version of it:

$$\mathcal{L}_S[H, y] := \frac{1}{m} \sum_{(x, y(x)) \in \mathcal{S}} \ell(H(x), y(x)), \quad (2)$$

or by minimizing $\mathcal{L}_S[H, y]$ along with additional regularization terms.

In contrast to the standard learning setting, in our framework we would like to learn a model $H = G \circ q \circ F$ that minimizes the expected risk, but also recovers the semantic attributes $f(x)$ (without any access to these features). Here, F and G are trainable representation function and classifier and q is a pre-defined discretization operator.

Put differently, the labels are given as proxy labels, while the actual goal is to learn a discrete-valued representation $q(F(x))$ of the data that maximizes some measure of feature fidelity $d_D(F) = d_D(f \| b \circ q \circ F)$ that depends on the distribution D and a binarization function b that translates a vector into a binary vector (see Sec. 5 for details).

3.1. Measures of Feature Fidelity

The goal of training in the proposed setting is to learn a representation of the data $q(F(x))$ that maximizes the fidelity of the extracted features with respect to an unseen set of ground-truth binary attributes $f(x)$.

In this section, we define a generic family of functions $d_D(f \| g)$ for measuring the fidelity of a multi-variate function $g : \mathcal{X} \rightarrow \mathcal{U}^d$ with respect to a multi-variate function $f : \mathcal{X} \rightarrow \mathcal{U}^n$ over a distribution D of samples.

Let $r(q_1, q_2; D)$ be a measure of accuracy between two univariate functions $q_1, q_2 : \mathcal{X} \rightarrow \mathcal{U}$ over a distribution D . For example, for binary functions, we can use the F1 score

(see below) or the accuracy rate $\mathbb{E}_{x \sim D} \{\mathbb{1}[q_1(x) = q_2(x)]\}$. Since we consider an unsupervised learning problem, we extend r to be annotation invariant by using $\hat{r}(q_1, q_2; D) := \max\{r(q_1, q_2; D), r(q_1, 1 - q_2; D)\}$ as a measure of accuracy which is invariant to whether positive samples are denoted by 1 or 0.

Let $g : \mathcal{X} \rightarrow \{0, 1\}^d$ and $f : \mathcal{X} \rightarrow \{0, 1\}^n$ be two multivariate binary functions. The fidelity of g with respect to f is defined in the following manner:

$$\begin{aligned} d_D(f \| g) &:= \max_{\pi: [n] \rightarrow [d]} \frac{1}{n} \sum_{i=1}^n \hat{r}(f_i, g_{\pi(i)}; D) \\ &= \frac{1}{n} \sum_{i=1}^n \max_{j \in [d]} \hat{r}(f_i, g_j; D) \end{aligned} \quad (3)$$

This quantity measures the average similarity between each feature f_i in f to some feature g_j in g . Informally, this quantity measures the extent at which the set of attributes in f can be treated as a subset of the set of attributes in g .

When measuring the fidelity over a finite set of test samples \mathcal{S}_T , the proposed $d_D(f \| g)$ considers the discrete uniform distribution $D = U[\mathcal{S}_T]$.

In this paper, since we focus on imbalanced multivariate binary functions f (i.e., $\mathcal{U} = \{0, 1\}$), r is chosen to be the F1 score. The F1 score is a measure of accuracy for imbalanced classification. For a given ground-truth binary function $q(x)$ and a classifier $p(x)$, the F1 score is calculated as the harmonic mean between the precision and recall of p with respect to q that are defined as follows:

$$\text{precision}(p, q) := \mathbb{P}_{x \sim D}[q(x) = 1 \mid p(x) = 1] \quad (4a)$$

$$\text{recall}(p, q) := \mathbb{P}_{x \sim D}[p(x) = 1 \mid q(x) = 1] \quad (4b)$$

Finally, in some cases, it is more relevant to measure the distance between f and g , instead of their similarity. We note that our method can be readily extended to this case by taking r to be a distance function and replacing the maximizations in Eq. (3) and the definition of \hat{r} by minimizations. For example, for real-valued functions (i.e., $\mathcal{U} \subset \mathbb{R}$), it is reasonable to use the distance between the two functions, $r(q_1, q_2; D) = \mathbb{E}_{x \sim D}[|q_1(x) - q_2(x)|]$.

4. Intersection Regularization

A key component of our method in Sec. 5 is the proposed notion of *Intersection Regularization*. In this section, we introduce and theoretically study the optimization dynamics of intersection regularization.

Suppose we have two hypothesis classes $\mathcal{G} = \{G_\theta \mid \theta \in \Theta\}$ and $\mathcal{T} = \{T_\omega \mid \omega \in \Omega\}$, where Θ and Ω are two sets of parameters. Intersection regularization involves solving the

following minimization problem:

$$\min_{\theta \in \Theta} \min_{\omega \in \Omega} \mathcal{Q}(\theta, \omega) \quad (5)$$

$$\text{where: } \mathcal{Q}(\theta, \omega) := \mathcal{L}_S[G_\theta, y] + \mathcal{L}_S[G_\theta, T_\omega]$$

In this problem, we are interested in learning a hypothesis $G_\theta \in \mathcal{G}$ that is closest to the target function y among all members of \mathcal{G} that can be approximated by a hypothesis $T_\omega \in \mathcal{T}$. We can think of \mathcal{T} as a prior knowledge we have on the target function y . Therefore, in some sense, the term $\mathcal{L}_S[G_\theta, T_\omega]$ acts as a regularization term that restricts G_θ to be close to the class \mathcal{T} .

In Sec. 5, we use intersection regularization to train a neural network G over a quantized representation that mimics a decision tree T and minimizes the classification error. In this case, the class \mathcal{T} consists of decision trees of a limited depth (ω is a vector that allocates an encoding of the tree, including its structure and decision rules) and \mathcal{G} is a class of neural networks of a fixed architecture (θ is a vector of the weights and biases of a given network). The underlying quantized representation thus obtained is suitable for classification by both a decision tree and a neural network.

The following analysis focuses on two main properties: finding a local minima of \mathcal{Q} and arriving at an equilibrium point of \mathcal{Q} . An equilibrium point of \mathcal{Q} is a pair (θ, ω) , such that, $\mathcal{Q}(\hat{\theta}, \hat{\omega}) = \min_{\theta} \mathcal{Q}(\theta, \hat{\omega}) = \min_{\omega} \mathcal{Q}(\hat{\theta}, \omega)$. The proofs are given in the supplementary material and are based on (cf. (Nesterov, 2014), Thm. 2.1.14) and the analysis of Song et al. (2017).

To study the convergence guarantees of this minimization problem, we make assumptions on the loss surface of \mathcal{Q} . Recall the following definitions.

Definition 1 (Convex function). *Let $f : \mathbb{R}^n \rightarrow \mathbb{R}$ be a differentiable function. We say that f is convex if for all $x, y \in \mathbb{R}^n$ and $t \in [0, 1]$ we have: $tf(x) + (1 - t)f(y) \geq f(tx + (1 - t)y)$.*

Definition 2 (Smooth function). *Let $f : \mathbb{R}^n \rightarrow \mathbb{R}$ be a differentiable function and $\beta > 0$. We say that f is β -smooth, if the gradient $\nabla f(x)$ is a β -Lipschitz function.*

Definition 3 (Critical and saddle points). *Let $f : \mathbb{R}^n \rightarrow \mathbb{R}$ be a differentiable function. A point x is critical for f if $\nabla f(x) = 0$. A critical point x is a saddle point if for all neighborhoods U around x , there are $a, b \in U$, such that, $f(a) \leq f(x) \leq f(b)$. A saddle point is strict, if the minimal eigenvalue of $\nabla^2 f(x)$ is negative.*

The following proposition shows that under certain conditions, it is possible to converge to an equilibrium of $\mathcal{Q}(\theta, \omega)$ when iteratively optimizing θ and ω . In order to show that, we assume that \mathcal{Q} is a convex function with respect to θ for any fixed value of ω . This is true, for example, when G_θ is a linear model. In addition, we assume that one is able to compute a global minimizer ω of $\mathcal{L}_S[G_\theta, T_\omega]$ for any θ . This

is typically impossible, however, it is reasonable to assume that one is able to approximately minimize $\mathcal{L}_{\mathcal{S}}[G_{\theta}, T_{\omega}]$ with respect to ω if the optimizer of ω is descent. Throughout the analysis, we assume that $\cup_{\omega \in \Omega} \arg \min_{\theta} \mathcal{Q}(\theta, \omega)$ is well-defined and bounded and that $\lim_{\theta: \|\theta\| \rightarrow \infty} \mathcal{L}_{\mathcal{S}}[G_{\theta}, y] = \infty$.

Proposition 1. *Assume that $\mathcal{Q}(\theta, \omega)$ is convex and β -smooth w.r.t θ for any fixed value of ω . Let θ_1 be some initialization and $\omega_1 \in \arg \min_{\omega} \mathcal{Q}(\theta_1, \omega)$. We define θ_t to be the weights produced after t iterations of applying Gradient Descent on $\mathcal{Q}(\theta, \omega_{t-1})$ over θ with learning rate $\mu < \beta^{-1}$ and $\omega_t = \arg \min_{\omega} \mathcal{Q}(\theta_{t-1}, \omega)$. Then, we have:*

$$\lim_{t \rightarrow \infty} \mathcal{Q}(\theta_t, \omega_t) = \lim_{t \rightarrow \infty} \min_{\theta} \mathcal{Q}(\theta, \omega_t) = \lim_{t \rightarrow \infty} \min_{\omega} \mathcal{Q}(\theta_t, \omega)$$

The following proposition shows that if we apply Block Coordinate Gradient Descent (BCGD) to optimize θ and ω for minimizing $\mathcal{Q}(\theta, \omega)$ (starting at (θ_1, ω_1)), then, they converge to a local minima that is also an equilibrium point. The BCGD iteratively updates: $\theta_{t+1} = \theta_t - \mu \nabla \mathcal{Q}(\theta_t, \omega_t)$ and $\omega_{t+1} = \omega_t - \mu \nabla \mathcal{Q}(\theta_{t+1}, \omega_t)$. Throughout the analysis we assume that the sets $\cup_{\omega \in \Omega} \arg \min_{\theta} \mathcal{Q}(\theta, \omega)$ and $\cup_{\theta \in \Theta} \arg \min_{\omega} \mathcal{Q}(\theta, \omega)$ are well-defined and bounded.

Proposition 2. *Assume that $\mathcal{Q}(\theta, \omega)$ is a twice-continuously differentiable, element-wise convex (i.e., convex w.r.t θ for any fixed value of ω and vice versa), Lipschitz continuous and β -smooth function, whose saddle points are strict. Let θ_t, ω_t be the weights produced after t iterations of applying BCGD on $\mathcal{Q}(\theta, \omega)$ with learning rate $\mu < \beta^{-1}$. (θ_t, ω_t) then converges to a local minima $(\hat{\theta}, \hat{\omega})$ of \mathcal{Q} that is also an equilibrium point.*

5. Method

In this section, we discuss propose our method for dealing with the problem introduced in Sec. 3.

Model Informally, our algorithm aims at learning a sparse discrete representation $F_q(x) := q(F(x))$ of the data, that is suitable for classification by a decision tree T of small depth. Intuitively, this leads to a representation that supports classification by relatively simple decision rules. For this purpose, we consider a model of the following form: $H_{tree} = T \circ F_q$, where $F : \mathcal{X} \rightarrow \mathbb{R}^d$ is a trainable neural network and $T : \mathbb{R}^d \rightarrow \mathbb{R}^k$ is a decision tree from a class \mathcal{T} of multivariate regression decision trees of maximal depth d_{max} . The function G (and T) is translated into a classifier by taking $\arg \max_{i \in [k]} G(F_q(x))$ (and $\arg \max_{i \in [k]} T(F_q(x))$).

In order to learn a neural network G that minimizes the classification error and also approximates a decision tree, we apply intersection regularization between a class of neural networks \mathcal{G} and the class of decision trees \mathcal{T} . Our objective function is decomposed into several loss functions. For each loss, we specify in brackets “[\cdot]” the components that are responsible for minimizing the specified loss functions. For a full description of our method, see Alg. 1.

Algorithm 1 Intersection Regularization based Sparse Attributes Recovery

Require: $\mathcal{S} = \{(x_i, y(x_i))\}_{i=1}^m$ - dataset; $\lambda_1, \lambda_2, \lambda_3$ - non-negative coefficients; I - number of epochs; s - batch size; A - Tree training algorithm (and splitting criteria);

- 1: Initialize F, G, T ;
- 2: Partition \mathcal{S} into batches $Batches(\mathcal{S})$ of size s ;
- 3: **for** $i = 1, \dots, I$ **do**
- 4: $U = \emptyset$;
- 5: $S' = \emptyset$;
- 6: **for** $B \in Batches(\mathcal{S})$ **do**
- 7: Initialize T ;
- 8: Let U be the x samples in B ;
- 9: Compute $V = \{(F_q(x), G(F_q(x))) \mid x \in U\}$ using uniform quantization;
- 10: Update $S' = S' \cup V$;
- 11: Train T over S' using A ;
- 12: Update G using GD to minimize $\mathcal{L}_B^1[F, G]$;
- 13: Update F using GD to minimize $\mathcal{L}_B^1[F, G] + \mathcal{L}_B^2[F]$;
- 14: **end for**
- 15: **end for**
- 16: **return** F, G, T ;

Our method partitions the dataset into batches $B = \{(x_i, y(x_i))\}_{i=1}^s$ of a fixed size (line 2 in Alg. 1) and iteratively optimizes the neural network and the decision tree. For each epoch (line 3), we iteratively update the network to minimize its objective function using GD and train the decision tree from scratch.

To optimize the neural network, we use three loss functions (lines 12-13). The first one is the cross-entropy loss of H_{net} with respect to the ground-truth labels, and the second one is the soft cross-entropy loss of H_{net} with respect to the probabilities of H_{tree} ,

$$\mathcal{L}_B^1[F, G] := \lambda_1 \mathcal{L}_B[H_{net}, y] + \lambda_2 \mathcal{L}_B[H_{net}, H_{tree}], \quad (6)$$

where the loss function $\ell : \Delta_k \times \Delta_k \rightarrow [0, \infty)$ is the cross-entropy loss that is defined as follows: $\ell(u, v) := -\sum_{i=1}^k v_i \cdot \log(u_i)$, k is the number of classes and Δ_k is the standard simplex.

To encourage sparse representations (Tibshirani, 1996; Koh et al., 2007), we also apply L_1 regularization over the quantized representation of the data. It is applied, at each training iteration, on a randomly selected subset of the features. This allows us to control the amount of regularization.

$$\mathcal{L}_B^2[F] := \frac{\lambda_3}{m} \sum_{i=1}^s \|F_q(x_i) \odot M\|_1, \quad (7)$$

where $M \in \{0, 1\}^d$ is a vector whose elements are sampled according to a Bernoulli random variable with parameter

$p \in (0, 1)$ and $\lambda_3 \geq 0$ is a predefined tradeoff parameter. Here, $u \odot v$ is the Hadamard product of $u, v \in \mathbb{R}^d$.

Tree Optimization During each epoch, we accumulate a dataset \mathcal{S}' of pairs $(F_q(x), G(F_q(x)))$ for all of the samples x that have been incurred until the current iteration (see lines 8-10 in Alg. 1). At each iteration, we train a multivariate regression decision tree T from scratch over the dataset \mathcal{S}' (see line 11 in Alg. 1). To train the decision tree, we used the CART algorithm (Loh, 2011) with the information gain splitting criteria.

Quantization and Binarization The function $F : \mathcal{X} \rightarrow \mathbb{R}^n$ is a real-valued multivariate function. To obtain a discrete representation of the data, we discretize the outputs of F using the uniform quantizer (Sheppard, 1897; Vanhoucke et al., 2011) q , see supplementary for the a step-by-step listing of the algorithm. This quantization employs a finite number of equally-sized bins. Their size is calculated by dividing the input range into 2^r bins, where r specifies the number of bits for encoding each bin.

Since the round function is non-differentiable, the gradients of the uniform quantization are usually approximated (Bengio et al., 2013; Ramapuram & Webb, 2019; Yang et al., 2019). In this paper, we utilize the straight-through estimator (STE) (Bengio et al., 2013), which assumes that the Jacobian of rounding is just identity, to estimate gradients of the discretization.

For applying the feature fidelity measure proposed in Sec. 3.1, we first cast the discrete vector $q(F(x))$ into a vector of binary features $b(q(F(x)))$ and compute $d_D(F) := d_D(f \| b \circ q \circ F)$, where b is a binarization function. In this paper, we use the following binarization scheme. For a given vector $v = q(F(x))$ we compute $u = b(v) := (u^1 \| u^2)$ as follows: for all $i \in [n]$ and $j \in [2^r]$, we have: $u_{i,j}^1 = \mathbb{1}[v_i = j]$ and $u_{i,j}^2 = \mathbb{1}[v_i \neq j]$, where $\mathbb{1}$ is the indicator function. The dimension of u is $2^{r+1} \cdot n$.

6. Experiments

In this section, we evaluate our method on several datasets with attributes in comparison with various baselines. To evaluate the attributes recovery quality, we use the evaluation metric explained in Sec. 3.1 based on the F1 score.

Implementation Details The architecture of the feature extractor F is taken from (Du et al., 2020) with the published hyperparameters, and is based on ResNet-50. The classifier G is a two-layered fully connected neural network with Mish activations (Misra, 2019). We initialize the ResNet with pretrained weights trained on ILSVRC2012 (Russakovsky et al., 2015). When training our method and the baselines we employed the following early stopping criteria: we train the model until the second epoch for which the accuracy rate drops over a validation set, and report the results on the

last epoch before the drop.

Throughout the experiments, we used the following default hyperparameters, except in our ablation studies, where we varied the hyperparameters to evaluate their effect. The coefficients for the loss functions $\lambda_1 = 2$, $\lambda_2 = 1$, $\lambda_3 = 0.001$. For the sparsity loss, we used Bernoulli random variables with parameter $p = 0.5$. The feature extractor F returns a vector of dimension 1024 and we use a 4-bits discretization. Optimization was carried out using SGD.

Datasets Throughout our experiments, we used the following datasets. (i) The aYahoo dataset (Farhadi et al., 2009), consisting of images from 12 classes (e.g., bag, goat, mug). Each image is labeled with 64 binary attributes. The images are collected from Yahoo. (ii) aPascal dataset (Farhadi et al., 2009) consisting of 20 classes of images. The images are labeled with the same 64 binary attributes as in the aYahoo dataset. (iii) Animals with attributes dataset (AwA2) (Xian et al., 2018) consisting of images from 50 animal classes, each class is labeled with 85 numeric attribute values, (iv) CUB-200-2011 (Wah et al., 2011) consisting of 200 bird species classes, each image is labeled with 312 binary attribute values.

Baseline methods We compare our method with various methods that capture a wide variety of approaches: (i) SDT (Frosst & Hinton, 2017) and ANT (Tanno et al., 2019), train a neural network of a tree architecture with the intention of learning high-level concepts. (ii) WS-DAN (Hu et al., 2019) is a method that generates attention maps to represent the object’s discriminative parts in order to improve the classification. (iii) DFL-CNN and Nts (Wang et al., 2018; Yang et al., 2018) use a network that captures class-specific discriminative regions. Region Grouping (Huang & Li, 2020) is a similar method that also uses a regularization term enforcing the empirical distribution of part occurrence to align a U-shaped prior distribution. (iv) ProtoPNet (Chen et al., 2019) computes similarity scores of informative patches in the image with learned prototype images. These similarity scores are then aggregated by an MLP classifier. All of the baselines, except ProtoPNet, are provided with labeled samples, without access to ground-truth semantic segmentation of any kind. In ProtoPNet they make use of cropping-based preprocessing that makes use of the bounding boxes provided with the CUB-200-2011 dataset.

To measure the baselines’ performance on our task, we apply quantization on the penultimate layer of each model. Since the larger the set of obtained features, the larger the mean fidelity score is expected to be, the comparison is done when fixing the representation layers dimensions and using the same quantization method. We, therefore, set the dimension of the penultimate in all baseline methods to be 1024 and apply uniform quantization with a 4 bits representation. This allows us to compute the fidelity score

Table 1. Comparing the performance of various baselines with our method. We report the classification accuracy rate (Acc) and the feature fidelity score ($d_D(F)$) for each method on each one of the datasets. For ProtoPNet on CUB-200-2011, we report the results with (right) and without (left) using cropping-based augmentations. As can be seen, our method outperforms the other methods in terms of recovering the semantic attributes across datasets.

Method	CUB-200-2011		aYahoo		Awa2		aPascal	
	Acc	$d_D(F)$	Acc	$d_D(F)$	Acc	$d_D(F)$	Acc	$d_D(F)$
SDT (Frosst & Hinton, 2017)	7.260%	17.00	16.38%	18.40	6.500%	45.19	30.48%	14.24
ANT (Tanno et al., 2019)	9.260%	18.52	45.16%	25.92	15.21%	18.22	37.00%	26.03
WS-DAN (Hu et al., 2019)	82.66%	26.14	95.54%	36.03	95.01%	61.35	76.67%	33.36
DFL-CNN (Wang et al., 2018)	83.92%	20.18	84.52%	16.33	87.12%	47.11	69.82%	20.06
Nts (Yang et al., 2018)	83.78%	27.07	96.50%	37.25	94.51%	59.78	82.11%	36.97
API-Net (Zhuang et al., 2020)	85.08%	28.07	97.00%	37.31	95.28%	66.32	78.36%	37.46
ProtoPNet (Chen et al., 2019)	42.0/77.5%	27.5/31.0	81.25%	36.79	87.52%	66.48	57.82%	34.98
Region Grouping (Huang & Li, 2020)	81.12%	26.95	88.79%	37.25	93.41%	66.75	68.56%	37.61
Quantized network	85.15%	23.27	97.20%	32.13	95.36%	61.80	82.54%	36.78
Quantized network + DT	35.75%	21.09	53.10%	29.42	46.25%	52.49	42.30%	27.58
Quantized network + L1	85.02%	29.71	96.47%	39.59	94.01%	67.53	80.16%	39.72
Our method	85.16%	32.25	95.47%	42.34	93.15%	70.65	80.03%	43.17

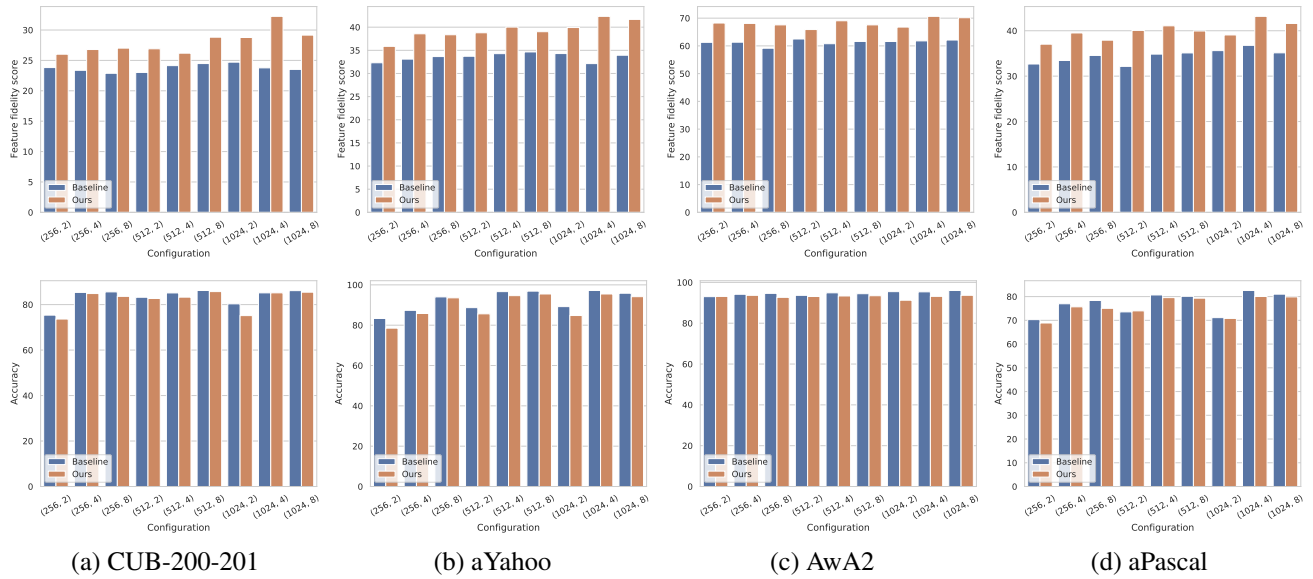


Figure 2. Comparing the performance of our method (orange) and a standard quantized neural network (blue). We compare the feature fidelity score ($d_D(F)$) (**top**) and the classification accuracy rate (**bottom**). We plot the results for different configurations of feature dimensions n and number of bits k for binarization. Each configuration is labeled with (n, k) .

of $q \circ F$ in the following manner $d_D(F) := d_D(f \| b \circ q \circ F)$, where F is the penultimate layer of the model.

6.1. Quantitative Analysis

In Tab. 1 we report the results of our method and the various baselines on each one of the datasets. As can be seen, our method has a significantly higher feature fidelity score, compared to the baselines across all datasets. We note that ProtoPNet (Chen et al., 2019) makes use of a cropping based preprocessing. In order to fairly compare its

results with the rest of the methods, we omitted using the preprocessing on all datasets except for CUB-200-2011, for which we report the results in both cases. As can be seen, our method achieves a fidelity score that is higher than ProtoPNet’s on CUB-200-2011, even though this kind of supervision helps ProtoPNet achieve the most competitive feature fidelity score among the baselines. On the other datasets, where no such crops were available, and ProtoPNet is trained on the entire frame, the feature fidelity score of ProtoPNet is significantly worse than that of our method.

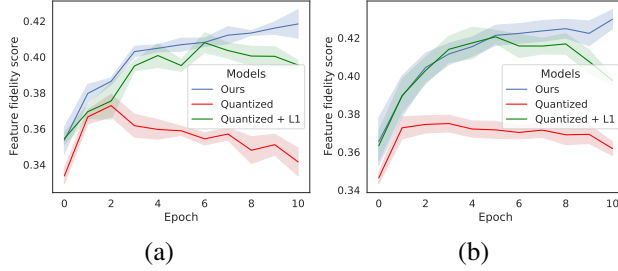


Figure 3. Comparing $d_D(F)$ during training. The x-axis stands for the epoch and the y-axis stands for the value of $d_D(F)$. (a) Results on aYahoo and (b) aPascal.

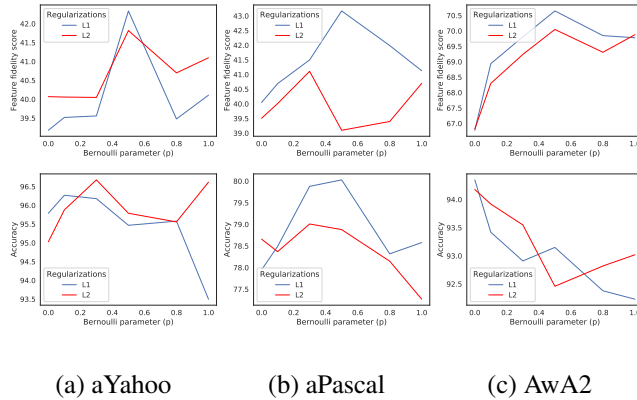


Figure 4. Comparing $d_D(F)$ (top) and the accuracy rate (bottom) when varying p for both L_1 and L_2 regularizations.

6.2. Ablation Studies

We conducted several ablation studies to validate the soundness of our method. Throughout the ablations, we compared our method with three of its variations: (i) a quantized network trained to minimize the cross-entropy loss, (ii) a quantized network trained to minimize the cross-entropy loss and the randomized L_1 regularization loss and (iii) a quantized network with a differentiable soft decision tree (SDT) on top of it, trained to minimize the cross-entropy loss. We used the online learning decision trees of [Dominigos & Hulten \(2000\)](#). In order to make the decision trees differentiable, we replaced the hard decision stamps with probabilistic decision stamps based on sigmoidal activations. The quantized network uses the same architecture as our model and is trained with the same hyperparameters. As can be seen in Tab. 1, our method significantly improves the recovery of the semantic attributes, at the small expense of a slight decrease in the classification accuracy, which is of second priority for our task.

Feature dimension and the number of bits To validate the sensitivity of our method to the size of obtained fea-

ture set, we compared it against a quantized neural network for different configurations of feature dimensions (in $\{256, 512, 1024\}$) and number of bits (in $\{2, 4, 8\}$). In Fig. 2, we report the fidelity score of each model, when averaged over 20 iterations. As can be seen, the fidelity of our method exceeds the fidelity of the baseline on each one of the configurations. On the other hand, the accuracy rate of both models is fairly similar for each configuration.

Number of epochs We compared the performance of the various methods as a function of training progress. In Fig. 3, we plot the averaged value of $d_D(F)$ (along with standard deviation) for each method when varying the number of training epochs. As can be seen, the performance of our method is monotonically increasing when increasing the number of epochs, as opposed to the alternative baselines. This demonstrates that apart from achieving a higher fidelity score, our regularization process also stabilizes the fidelity score. We note that without access to the ground-truth attributes, we cannot measure $d_D(F)$, and therefore, we cannot decide when to stop based on the value of $d_D(F)$. An algorithm that monotonically increases the value of $d_D(F)$ during training, allows us to safely stop training after a sufficient number of epochs.

Randomized regularization To study the regularization term, we ran our method when varying the value of $p \in \{0, 0.1, 0.3, 0.5, 0.8, 1\}$ for the L_1 regularization over the quantized features (Eq. 7). This was repeated for L_2 regularization (i.e., replacing $\|\cdot\|_1$ with $\|\cdot\|_2^2$). As can be seen in Fig. 4, the performance of our method is better when using the L_1 regularization. In addition, the value of p has a significant effect on the results. Specifically, the results are worse when the regularization is almost never present (small p) or present for almost all variable (large p).

7. Conclusions

In this paper, we introduced the problem of ‘‘Unsupervised Recovery of Semantic Attributes’’. This problem explores the emergence of interpretable features in a quantitative way, based on a set of semantic features that is unseen during training. We present evidence that methods that are tailored to extract semantic attributes do not necessarily perform well in this metric and suggest a new method. Our method is based on learning, concurrently, in the soft-intersection of two hypothesis classes: a neural network for obtaining its classification power, and a decision tree in order to learn features that lend themselves to classification by short logical expressions. We demonstrate that learning this way is more effective than other methods for the new task and that learning with the new regularization scheme improves the fidelity of the obtained feature map.

References

- Alvarez-Melis, D. and Jaakkola, T. S. Towards robust interpretability with self-explaining neural networks. In Bengio, S., Wallach, H., Larochelle, H., Grauman, K., Cesa-Bianchi, N., and Garnett, R. (eds.), *Advances in Neural Information Processing Systems*, volume 31, pp. 7775–7784. Curran Associates, Inc., 2018a.
- Alvarez-Melis, D. and Jaakkola, T. S. On the robustness of interpretability methods. *arXiv preprint arXiv:1806.08049*, 2018b.
- Asano, Y. M., Rupprecht, C., and Vedaldi, A. A critical analysis of self-supervision, or what we can learn from a single image. *arXiv preprint arXiv:1904.13132*, 2019.
- Bach, S., Binder, A., Montavon, G., Klauschen, F., Müller, K.-R., and Samek, W. On pixel-wise explanations for non-linear classifier decisions by layer-wise relevance propagation. *PLoS one*, 10(7):e0130140, 2015.
- Bengio, Y., Léonard, N., and Courville, A. C. Estimating or propagating gradients through stochastic neurons for conditional computation. *CoRR*, abs/1308.3432, 2013.
- Chen, C., Li, O., Barnett, A., Su, J., and Rudin, C. This looks like that: deep learning for interpretable image recognition. In *NeurIPS*, 2019.
- Dabkowski, P. and Gal, Y. Real time image saliency for black box classifiers. In *Advances in Neural Information Processing Systems*, pp. 6970–6979, 2017.
- Domingos, P. and Hulten, G. Mining high-speed data streams. In *Proceedings of the Sixth ACM SIGKDD International Conference on Knowledge Discovery and Data Mining*, KDD '00, pp. 71–80, New York, NY, USA, 2000. Association for Computing Machinery. ISBN 1581132336.
- Du, R., Chang, D., Bhunia, A. K., Xie, J., Ma, Z., Song, Y.-Z., and Guo, J. Fine-grained visual classification via progressive multi-granularity training of jigsaw patches. In *European Conference on Computer Vision*, pp. 153–168. Springer, 2020.
- Erhan, D., Bengio, Y., Courville, A., and Vincent, P. Visualizing higher-layer features of a deep network. *University of Montreal*, 1341(3):1, 2009.
- Farhadi, A., Endres, I., Hoiem, D., and Forsyth, D. Describing objects by their attributes. In *2009 IEEE Conference on Computer Vision and Pattern Recognition*, pp. 1778–1785. IEEE, 2009.
- Fong, R., Patrick, M., and Vedaldi, A. Understanding deep networks via extremal perturbations and smooth masks. In *Proceedings of the IEEE International Conference on Computer Vision*, pp. 2950–2958, 2019.
- Fong, R. C. and Vedaldi, A. Interpretable explanations of black boxes by meaningful perturbation. In *Proceedings of the IEEE International Conference on Computer Vision*, pp. 3429–3437, 2017.
- Frosst, N. and Hinton, G. Distilling a neural network into a soft decision tree. *arXiv preprint arXiv:1711.09784*, 2017.
- Gu, J., Yang, Y., and Tresp, V. Understanding individual decisions of cnns via contrastive backpropagation. In *Asian Conference on Computer Vision*, pp. 119–134. Springer, 2018.
- Guidotti, R., Monreale, A., Ruggieri, S., Turini, F., Giannotti, F., and Pedreschi, D. A survey of methods for explaining black box models. *ACM computing surveys (CSUR)*, 51(5):1–42, 2018.
- Gur, S., Ali, A., and Wolf, L. Visualization of supervised and self-supervised neural networks via attribution guided factorization. *arXiv preprint arXiv:2012.02166*, 2020.
- Herbarium, J. Jepson manual e-flora. URL: <http://ucjeps.berkeley.edu/>(accessed 18 Jan 2013). Berkeley (CA): University of California, Berkeley, 2013.
- Hu, T., Qi, H., Huang, Q., and Lu, Y. See better before looking closer: Weakly supervised data augmentation network for fine-grained visual classification, 2019.
- Huang, Z. and Li, Y. Interpretable and accurate fine-grained recognition via region grouping. In *CVPR*, pp. 8662–8672, 2020.
- Hubara, I., Courbariaux, M., Soudry, D., El-Yaniv, R., and Bengio, Y. Quantized neural networks: Training neural networks with low precision weights and activations. *Journal of Machine Learning Research*, 18(187):1–30, 2018.
- Irsoy, O., Yildiz, O. T., and Alpaydin, E. Soft decision trees. In *International Conference on Pattern Recognition*, 2012.
- Iwana, B. K., Kuroki, R., and Uchida, S. Explaining convolutional neural networks using softmax gradient layer-wise relevance propagation. *arXiv preprint arXiv:1908.04351*, 2019.
- Koh, K., Kim, S.-J., and Boyd, S. An interior-point method for large-scale ℓ_1 -regularized logistic regression. *Journal of Machine Learning Research*, 8(54):1519–1555, 2007.
- Li, K., Wu, Z., Peng, K.-C., Ernst, J., and Fu, Y. Tell me where to look: Guided attention inference network. In *Proceedings of the IEEE Conference on Computer Vision and Pattern Recognition*, pp. 9215–9223, 2018.

- Loh, W.-Y. Classification and regression trees. *Wiley interdisciplinary reviews: data mining and knowledge discovery*, 1(1):14–23, 2011.
- Lundberg, S. M. and Lee, S.-I. A unified approach to interpreting model predictions. In *Advances in Neural Information Processing Systems*, pp. 4765–4774, 2017.
- Mahendran, A. and Vedaldi, A. Visualizing deep convolutional neural networks using natural pre-images. *International Journal of Computer Vision*, 120(3):233–255, 2016.
- Misra, D. Mish: A self regularized non-monotonic neural activation function. *arXiv preprint arXiv:1908.08681*, 4, 2019.
- Montavon, G., Lapuschkin, S., Binder, A., Samek, W., and Müller, K.-R. Explaining nonlinear classification decisions with deep taylor decomposition. *Pattern Recognition*, 65:211–222, 2017.
- Nam, W.-J., Gur, S., Choi, J., Wolf, L., and Lee, S.-W. Relative attributing propagation: Interpreting the comparative contributions of individual units in deep neural networks. *arXiv preprint arXiv:1904.00605*, 2019.
- Nesterov, Y. *Introductory Lectures on Convex Optimization: A Basic Course*. Springer Publishing Company, Incorporated, 1 edition, 2014. ISBN 1461346916.
- Ramapuram, J. and Webb, R. Improving discrete latent representations with differentiable approximation bridges, 2019.
- Ribeiro, M. T., Singh, S., and Guestrin, C. “Why should I trust you?”: Explaining the predictions of any classifier. In *Proceedings of the 22Nd ACM SIGKDD International Conference on Knowledge Discovery and Data Mining, KDD ’16*, pp. 1135–1144, New York, NY, USA, 2016. ACM. ISBN 978-1-4503-4232-2.
- Russakovsky, O., Deng, J., Su, H., Krause, J., Satheesh, S., Ma, S., Huang, Z., Karpathy, A., Khosla, A., Bernstein, M., Berg, A. C., and Fei-Fei, L. Imagenet large scale visual recognition challenge. *Int. J. Comput. Vision*, 115(3):211–252, December 2015.
- Selvaraju, R. R., Cogswell, M., Das, A., Vedantam, R., Parikh, D., and Batra, D. Grad-cam: Visual explanations from deep networks via gradient-based localization. In *Proceedings of the IEEE international conference on computer vision*, pp. 618–626, 2017.
- Sheppard, W. F. On the calculation of the most probable values of frequency-constants, for data arranged according to equidistant division of a scale. *Proceedings of the London Mathematical Society*, 1(1):353–380, 1897.
- Shrikumar, A., Greenside, P., Shcherbina, A., and Kundaje, A. Not just a black box: Learning important features through propagating activation differences. *arXiv preprint arXiv:1605.01713*, 2016.
- Shulman, E. and Wolf, L. Meta decision trees for explainable recommendation systems. In *Proceedings of the AAAI/ACM Conference on AI, Ethics, and Society, AIES ’20*, pp. 365–371, New York, NY, USA, 2020. Association for Computing Machinery. ISBN 9781450371100.
- Simonyan, K., Vedaldi, A., and Zisserman, A. Deep inside convolutional networks: Visualising image classification models and saliency maps. *arXiv preprint arXiv:1312.6034*, 2013.
- Smilkov, D., Thorat, N., Kim, B., Viégas, F., and Wattenberg, M. Smoothgrad: removing noise by adding noise. *arXiv preprint arXiv:1706.03825*, 2017.
- Song, E., Shen, Z., and Shi, Q. Block coordinate descent only converge to minimizers, 2017.
- Srinivas, S. and Fleuret, F. Full-gradient representation for neural network visualization. In *Advances in Neural Information Processing Systems*, pp. 4126–4135, 2019.
- Stokes, P. Computer-aided palaeography, present and future. In Rehbein, M., Schaßan, T., and Sahle, P. (eds.), *Kodikologie und Paläographie im digitalen Zeitalter - Codicology and Palaeography in the Digital Age*, volume 2, pp. 309–338. BoD, Norderstedt, 2009.
- Sundararajan, M., Taly, A., and Yan, Q. Axiomatic attribution for deep networks. In *Proceedings of the 34th International Conference on Machine Learning-Volume 70*, pp. 3319–3328. JMLR. org, 2017.
- Tanno, R., Arulkumaran, K., Alexander, D., Criminisi, A., and Nori, A. Adaptive neural trees. In Chaudhuri, K. and Salakhutdinov, R. (eds.), *Proceedings of the 36th International Conference on Machine Learning*, volume 97 of *Proceedings of Machine Learning Research*, pp. 6166–6175. PMLR, 09–15 Jun 2019.
- Tibshirani, R. Regression shrinkage and selection via the lasso. *Journal of the Royal Statistical Society. Series B (Methodological)*, 58(1):267–288, 1996.
- Vanhoucke, V., Senior, A., and Mao, M. Z. Improving the speed of neural networks on cpus. In *Deep Learning and Unsupervised Feature Learning Workshop, NIPS 2011*, 2011.
- Wah, C., Branson, S., Welinder, P., Perona, P., and Belongie, S. The Caltech-UCSD Birds-200-2011 Dataset. Technical Report CNS-TR-2011-001, Caltech, 2011.

Wang, Y., Morariu, V. I., and Davis, L. S. Learning a discriminative filter bank within a CNN for fine-grained recognition. In *Proceedings of the IEEE Conference on Computer Vision and Pattern Recognition (CVPR)*, June 2018.

Xian, Y., Lampert, C. H., Schiele, B., and Akata, Z. Zero-shot learning—a comprehensive evaluation of the good, the bad and the ugly. *IEEE Transactions on Pattern Analysis and Machine Intelligence*, 41(9):2251–2265, 2018.

Xu, W., Wang, J., Wang, Y., Wu, Y., and Akata, Z. Generating visual and semantic explanations with multi-task network. In *European Conference on Computer Vision*, pp. 620–635. Springer, 2020.

Yang, J., Shen, X., Xing, J., Tian, X., Li, H., Deng, B., Huang, J., and Hua, X.-s. Quantization networks. In *Proceedings of the IEEE/CVF Conference on Computer Vision and Pattern Recognition (CVPR)*, June 2019.

Yang, Z., Luo, T., Wang, D., Hu, Z., Gao, J., and Wang, L. Learning to navigate for fine-grained classification, 2018.

Yeh, C.-K., Hsieh, C.-Y., Suggala, A. S., Inouye, D., and Ravikumar, P. How sensitive are sensitivity-based explanations? *arXiv preprint arXiv:1901.09392*, 2019.

Zeiler, M. D. and Fergus, R. Visualizing and understanding convolutional networks. In *European conference on computer vision*, pp. 818–833. Springer, Cham, 2014.

Zhang, J., Bargal, S. A., Lin, Z., Brandt, J., Shen, X., and Sclaroff, S. Top-down neural attention by excitation backprop. *International Journal of Computer Vision*, 126(10):1084–1102, 2018.

Zhang, N., Paluri, M., Ranzato, M., Darrell, T., and Bourdev, L. Panda: Pose aligned networks for deep attribute modeling. In *Proceedings of the IEEE conference on computer vision and pattern recognition*, pp. 1637–1644, 2014.

Zhou, B., Khosla, A., Lapedriza, A., Oliva, A., and Torralba, A. Learning deep features for discriminative localization. In *Proceedings of the IEEE conference on computer vision and pattern recognition*, pp. 2921–2929, 2016a.

Zhou, B., Bau, D., Oliva, A., and Torralba, A. Interpreting deep visual representations via network dissection. *IEEE transactions on pattern analysis and machine intelligence*, 2018.

Zhou, S., Wu, Y., Ni, Z., Zhou, X., Wen, H., and Zou, Y. Dorefa-net: Training low bitwidth convolutional neural networks with low bitwidth gradients. *arXiv preprint arXiv:1606.06160*, 2016b.

Algorithm 2 The uniform quantization method (forward and backward passes)

Require: x is tensor to be quantized; r number of bits.

- 1: $q_{\min}, q_{\max} = 0, 2^r - 1$;
- 2: $x_{\min}, x_{\max} = \min_j \{x_j\}, \max_j \{x_j\}$;
- 3: $s = \frac{x_{\max} - x_{\min}}{q_{\max} - q_{\min}}$;
- 4: $z_{\text{init}} = \frac{q_{\min} - x_{\min}}{s}$;
- 5: $z = \min(\max(z_{\text{init}}, q_{\min}), q_{\max})$;
- 6: $\tilde{z} = \text{round}(z)$;
- 7: $\forall i: \tilde{q}_i = \tilde{z} + \frac{x_i}{s}$;
- 8: $\forall i: q_i = \text{round}(\min(\max(\tilde{q}_i, q_{\min}), q_{\max}))$;
- 9: $\partial \tilde{z} = \mathbb{1}[z_{\text{init}} \in (q_{\min}, q_{\max})] \cdot \frac{\partial z_{\text{init}}}{\partial x}$;
- 10: $\forall i: \partial \tilde{q}_i = \partial \tilde{z} + \frac{\partial(x_i/s)}{\partial x}$;
- 11: $\forall i: \partial q_i = \mathbb{1}[\tilde{q}_i \in (q_{\min}, q_{\max})] \cdot \partial \tilde{q}_i$;
- 12: **return** $q, \partial q$;

Zhuang, P., Wang, Y., and Qiao, Y. Learning attentive pairwise interaction for fine-grained classification. In *AAAI*, pp. 13130–13137, 2020.

A. Uniform Quantization

The uniform quantization method is fully described in Alg. 2. For a given function p , we denote by ∂p the estimated gradients of p w.r.t x . In Alg. 2, the estimated gradient of \tilde{z} is computed as the gradient of $\min(\max(z_{\text{init}}, q_{\min}), q_{\max})$ (since $\partial \text{round}(x) = 1$ when applying STE (Bengio et al., 2013)), which is simply $\mathbb{1}[z_{\text{init}} \in (q_{\min}, q_{\max})] \cdot \frac{\partial z_{\text{init}}}{\partial x}$, where $\frac{\partial z_{\text{init}}}{\partial x}$ is the gradient of z_{init} w.r.t x . $\partial \tilde{q}_i$ and ∂q are defined similarly, see lines 10-11 in Alg. 2.

B. Additional Experimental Details

Datasets The aYahoo dataset (Farhadi et al., 2009) consists of 1850 training images and 794 test images, (ii) aPascal dataset (Farhadi et al., 2009) has 2869 training images and 2227 test images, (iii) Awa2 (Xian et al., 2018) we used 26125 training images and 11197 test images, (iv) CUB-200-2011 (Wah et al., 2011) contains 5994 training images and 5794 test images. We used the standard train/test splits for each one of the datasets, except Awa2, where we follow a 0.7/0.3 random split because there is no standard partition for this dataset.

Runtime and Infrastructure The experiments were run on three GeForce RTX 3090 GPUs. Our method completes an epoch every 7 minutes on aYahoo, 10 minutes on aPascal, 1 hours on Awa2 and 1 hours on CUB-200-2011. On average our method runs for approximately 12 epochs on both aYahoo and aPascal, 2-4 epochs on Awa2 and 35-40 on CUB-200-2011.

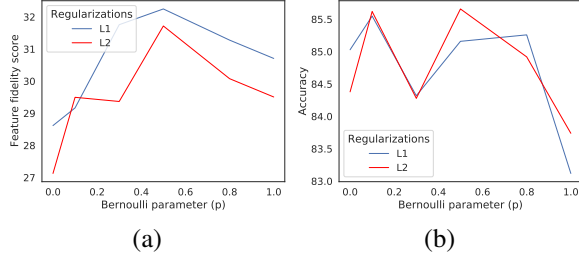


Figure 5. Comparing $d_D(F)$ (a) and the accuracy rate (b) when varying p for both L_1 and L_2 regularizations.

C. Additional Experiments

In Fig. 5 we plot the results of the same experiment as in Fig. 4 in the main text for the CUB-200-2011 (Wah et al., 2011) dataset. These results conform with the observations summarized in the main text.

D. Proofs of Props. 1 and 2

Proposition 1. Assume that $\mathcal{Q}(\theta, \omega)$ is convex and β -smooth w.r.t θ for any fixed value of ω . Let θ_1 be some initialization and $\omega_1 \in \arg \min_{\omega} \mathcal{Q}(\theta_1, \omega)$. We define θ_t to be the weights produced after t iterations of applying Gradient Descent on $\mathcal{Q}(\theta, \omega_{t-1})$ over θ with learning rate $\mu < \beta^{-1}$ and $\omega_t = \arg \min_{\omega} \mathcal{Q}(\theta_{t-1}, \omega)$. Then, we have:

$$\lim_{t \rightarrow \infty} \mathcal{Q}(\theta_t, \omega_t) = \lim_{t \rightarrow \infty} \min_{\theta} \mathcal{Q}(\theta, \omega_t) = \lim_{t \rightarrow \infty} \min_{\omega} \mathcal{Q}(\theta_t, \omega)$$

Proof. First, we would like to prove that $\mathcal{Q}(\theta_t, \omega_t)$ is monotonically decreasing. We notice that for each $t \in \mathbb{N}$, we have:

$$\mathcal{Q}(\theta_t, \omega_t) \leq \mathcal{Q}(\theta_t, \omega_{t-1}) \quad (8)$$

since ω_t is the global minimizer of $\mathcal{Q}(\theta_t, \omega)$. In addition, by the proof of (cf. Nesterov (2014), Thm. 2.1.14), we have:

$$\begin{aligned} \mathcal{Q}(\theta_t, \omega_{t-1}) &\leq \mathcal{Q}(\theta_{t-1}, \omega_{t-1}) \\ &\quad - \eta \|\nabla_{\theta} \mathcal{Q}(\theta_{t-1}, \omega_{t-1})\|_2^2 \\ &\leq \mathcal{Q}(\theta_{t-1}, \omega_{t-1}), \end{aligned} \quad (9)$$

where $\eta := \mu(1 - 0.5\beta\mu) > 0$. Therefore, we conclude that $\mathcal{Q}(\theta_t, \omega_t)$ is indeed monotonically decreasing. Since \mathcal{Q} is non-negative, we conclude that $\mathcal{Q}(\theta_t, \omega_t)$ is a convergent sequence. In particular, θ_t is bounded. Otherwise, $\mathcal{Q}(\theta_t, \omega_t) \geq \mathcal{L}_S[h_{\theta_t}, y] \rightarrow \infty$ in contradiction to the fact that $\mathcal{Q}(\theta_t, \omega_t)$ is a convergent sequence.

Next, by applying the convexity of $\mathcal{Q}(\theta, \omega_{t-1})$ (as a function of θ), we have:

$$\begin{aligned} &\mathcal{Q}(\theta_t, \omega_{t-1}) - \mathcal{Q}(\theta_t^*, \omega_{t-1}) \\ &\leq \langle \nabla_{\theta} \mathcal{Q}(\theta, \omega_{t-1}), \theta_t - \theta_t^* \rangle \\ &\leq \|\nabla_{\theta} \mathcal{Q}(\theta, \omega_{t-1})\|_2 \cdot \|\theta_t - \theta_t^*\|_2, \end{aligned} \quad (10)$$

where $\theta_t^* = \arg \min_{\theta} \mathcal{Q}(\theta, \omega_t)$. By combining Eqs. (9) and (10), we have:

$$\begin{aligned} &\mathcal{Q}(\theta_t, \omega_t) \\ &\leq \mathcal{Q}(\theta_t, \omega_{t-1}) \leq \mathcal{Q}(\theta_{t-1}, \omega_{t-1}) \\ &\quad - \frac{\eta}{\|\theta_t - \theta_t^*\|_2^2} \left(\mathcal{Q}(\theta_{t-1}, \omega_{t-1}) - \min_{\theta} \mathcal{Q}(\theta, \omega_{t-1}) \right)^2 \end{aligned} \quad (11)$$

In particular,

$$\begin{aligned} &\mathcal{Q}(\theta_{t-1}, \omega_{t-1}) - \mathcal{Q}(\theta_t, \omega_t) \\ &\geq \frac{\eta}{\|\theta_t - \theta_t^*\|_2^2} \left(\mathcal{Q}(\theta_{t-1}, \omega_{t-1}) - \min_{\theta} \mathcal{Q}(\theta, \omega_{t-1}) \right)^2 \end{aligned} \quad (12)$$

Since the left hand side tends to zero and the right hand side is lower bounded by zero, by the sandwich theorem, the right hand side tends to zero as well. Since both θ_t and θ_t^* are bounded sequences ($\{\arg \min_{\theta} \mathcal{Q}(\theta, \omega) \mid \omega \in \Omega\}$ is well-defined and bounded), we conclude that $\lim_{t \rightarrow \infty} \mathcal{Q}(\theta_t, \omega_t) = \lim_{t \rightarrow \infty} \min_{\theta} \mathcal{Q}(\theta, \omega_t)$. We also have: $\mathcal{Q}(\theta_t, \omega_t) = \min_{\omega} \mathcal{Q}(\theta_t, \omega)$ by definition, and therefore, $\lim_{t \rightarrow \infty} \mathcal{Q}(\theta_t, \omega_t) = \lim_{t \rightarrow \infty} \min_{\omega} \mathcal{Q}(\theta_t, \omega)$ as well. \square

Proposition 2. Assume that $\mathcal{Q}(\theta, \omega)$ is a twice-continuously differentiable, element-wise convex (i.e., convex w.r.t θ for any fixed value of ω and vice versa), Lipschitz continuous and β -smooth function, whose saddle points are strict. Let θ_t, ω_t be the weights produced after t iterations of applying BCGD on $\mathcal{Q}(\theta, \omega)$ with learning rate $\mu < \beta^{-1}$. (θ_t, ω_t) then converges to a local minima $(\hat{\theta}, \hat{\omega})$ of \mathcal{Q} that is also an equilibrium point.

Proof. Firstly, since $\mathcal{Q}(\theta, \omega)$ is a twice-continuously differentiable, Lipschitz continuous and β -smooth function, by Prop. 3.4 and Cor. 3.1 in (Song et al., 2017), (θ_t, ω_t) converge to a local minima $(\hat{\theta}, \hat{\omega})$ of \mathcal{Q} . Therefore, it is left to show that $(\hat{\theta}, \hat{\omega})$ is also an equilibrium point. We note that $\mathcal{Q}(\theta, \omega)$ is element-wise convex and β -smooth. By the proof of (cf. Nesterov (2014), Thm. 2.1.14), we have:

$$\begin{aligned} &\mathcal{Q}(\theta_{t+1}, \omega_t) \\ &\leq \mathcal{Q}(\theta_t, \omega_t) - \eta \|\nabla_{\theta} \mathcal{Q}(\theta_t, \omega_t)\|_2^2, \end{aligned} \quad (13)$$

where $\eta := \mu(1 - 0.5\beta\mu) > 0$. By applying the convexity of $\mathcal{Q}(\theta, \omega_t)$ (as a function of θ), we have:

$$\begin{aligned} &\mathcal{Q}(\theta_t, \omega_t) - \mathcal{Q}(\theta_t^*, \omega_t) \\ &\leq \langle \nabla_{\theta} \mathcal{Q}(\theta, \omega_t), \theta_t - \theta_t^* \rangle \\ &\leq \|\nabla_{\theta} \mathcal{Q}(\theta_t, \omega_t)\|_2 \cdot \|\theta_t - \theta_t^*\|_2, \end{aligned} \quad (14)$$

where $\theta_t^* = \arg \min_{\theta} \mathcal{Q}(\theta, \omega_t)$ and $\omega_t^* = \arg \min_{\omega} \mathcal{Q}(\theta_{t+1}, \omega)$. By combining Eqs. (13) and (14),

we have:

$$\begin{aligned} \mathcal{Q}(\theta_{t+1}, \omega_t) &\leq \mathcal{Q}(\theta_t, \omega_t) \\ &- \frac{\eta}{\|\theta_t - \theta_t^*\|_2^2} \left(\mathcal{Q}(\theta_t, \omega_t) - \min_{\theta} \mathcal{Q}(\theta, \omega_t) \right)^2 \end{aligned} \quad (15)$$

and similarly, we have:

$$\begin{aligned} \mathcal{Q}(\theta_{t+1}, \omega_{t+1}) &\leq \mathcal{Q}(\theta_{t+1}, \omega_t) \\ &- \frac{\eta}{\|\omega_t - \omega_t^*\|_2^2} \left(\mathcal{Q}(\theta_{t+1}, \omega_t) - \min_{\omega} \mathcal{Q}(\theta_{t+1}, \omega) \right)^2 \end{aligned} \quad (16)$$

In particular, we have:

$$\begin{aligned} &\mathcal{Q}(\theta_{t+1}, \omega_{t+1}) \\ &\leq \mathcal{Q}(\theta_t, \omega_t) \\ &- \frac{\eta}{\|\theta_t - \theta_t^*\|_2^2} \left(\mathcal{Q}(\theta_t, \omega_t) - \min_{\theta} \mathcal{Q}(\theta, \omega_t) \right)^2 \\ &- \frac{\eta}{\|\omega_t - \omega_t^*\|_2^2} \left(\mathcal{Q}(\theta_{t+1}, \omega_t) - \min_{\omega} \mathcal{Q}(\theta_{t+1}, \omega) \right)^2 \end{aligned} \quad (17)$$

Therefore, the sequence $\mathcal{Q}(\theta_t, \omega_t)$ is monotonically decreasing. Since $\mathcal{Q}(\theta_t, \omega_t)$ is non-negative, it converges to some non-negative constant. By Eq. (17), we have:

$$\begin{aligned} &\mathcal{Q}(\theta_{t+1}, \omega_{t+1}) - \mathcal{Q}(\theta_t, \omega_t) \\ &\geq \frac{\eta}{\|\theta_t - \theta_t^*\|_2^2} \left(\mathcal{Q}(\theta_t, \omega_t) - \min_{\theta} \mathcal{Q}(\theta, \omega_t) \right)^2 \\ &+ \frac{\eta}{\|\omega_t - \omega_t^*\|_2^2} \left(\mathcal{Q}(\theta_{t+1}, \omega_t) - \min_{\omega} \mathcal{Q}(\theta_{t+1}, \omega) \right)^2 \end{aligned} \quad (18)$$

Since the left hand side tends to zero and the right hand side is lower bounded by zero, by the sandwich theorem, the sequences $\frac{\eta}{\|\theta_t - \theta_t^*\|_2^2} \left(\mathcal{Q}(\theta_t, \omega_t) - \min_{\theta} \mathcal{Q}(\theta, \omega_t) \right)^2$ and $\frac{\eta}{\|\omega_t - \omega_t^*\|_2^2} \left(\mathcal{Q}(\theta_{t+1}, \omega_t) - \min_{\omega} \mathcal{Q}(\theta_{t+1}, \omega) \right)^2$ tend to zero. We note that θ_t and ω_t are convergent sequences, and therefore, are bounded as well. In addition, we recall that the sets $\{\arg \min_{\theta} \mathcal{Q}(\theta, \omega) \mid \omega \in \Omega\}$ and $\{\arg \min_{\omega} \mathcal{Q}(\theta, \omega) \mid \theta \in \Theta\}$ are well-defined and bounded. Hence, the terms $\|\theta_t - \theta_t^*\|_2^2$ and $\|\omega_t - \omega_t^*\|_2^2$ are bounded. Thus, we conclude that the sequences $\left(\mathcal{Q}(\theta_t, \omega_t) - \min_{\theta} \mathcal{Q}(\theta, \omega_t) \right)^2$ and $\left(\mathcal{Q}(\theta_{t+1}, \omega_t) - \min_{\omega} \mathcal{Q}(\theta_{t+1}, \omega) \right)^2$ tend to zero. In particular,

$$\begin{aligned} \lim_{t \rightarrow \infty} \mathcal{Q}(\theta_t, \omega_t) &= \lim_{t \rightarrow \infty} \min_{\theta} \mathcal{Q}(\theta, \omega_t) \\ \lim_{t \rightarrow \infty} \mathcal{Q}(\theta_{t+1}, \omega_t) &= \lim_{t \rightarrow \infty} \min_{\omega} \mathcal{Q}(\theta_t, \omega) \end{aligned} \quad (19)$$

Since \mathcal{Q} is a Lipschitz continuous function, we have: (i) $\lim_{t \rightarrow \infty} \mathcal{Q}(\theta_{t+1}, \omega_t) = \lim_{t \rightarrow \infty} \mathcal{Q}(\theta_t, \omega_t) = \mathcal{Q}(\hat{\theta}, \hat{\omega})$, (ii) $\lim_{t \rightarrow \infty} \min_{\theta} \mathcal{Q}(\theta, \omega_t) = \min_{\theta} \mathcal{Q}(\theta, \hat{\omega})$ and (iii) $\lim_{t \rightarrow \infty} \min_{\omega} \mathcal{Q}(\theta_t, \omega) = \min_{\omega} \mathcal{Q}(\hat{\theta}, \omega)$. Therefore, we finally conclude that $(\hat{\theta}, \hat{\omega})$ is an equilibrium point of \mathcal{Q} . \square